A 24x7 Perovskite Catalyst through Oxygen Vacancy Engineering for Rapid Catalytic Degradation of Azo Dyes under Dark and Ambient Light

Suruthi Rajendran[a,1], Dhakshnamoorthi Harikaran[a,1], Vijayaraghavan R[a,*]

[a] *Department of Chemistry, School of Advanced Sciences, Vellore Institute of Technology, Vellore -632 014, India.*

[*]Corresponding author: rvijayaraghavan@vit.ac.in

[1]*Authors of equal contribution*

Text S1. Synthesis of $BaSn_{1-x}Cu_xO_3$ by the solid-state method

Materials used:

- Barium carbonate ($BaCO_3$) 99.9% - SDFCL
- Tin oxide (SnO_2) 99.9% - SDFCL
- Copper oxide (CuO) 99.9% - SDFCL

Procedure:

Cu-doped $BaSnO_3$ perovskite oxides were synthesized via a conventional solid-state synthesis (SSS) route. Stoichiometric amounts of $BaCO_3$, SnO_2, and CuO were weighed according to the desired composition (x = 0.05, 0.10, 0.15, and 0.20, where x denotes the molar fraction of Cu substituting Sn). The precursor powders were thoroughly ground in a mortar and pestle for 30 min to ensure homogeneous mixing. The mixtures were calcined at 1200 °C for 12 h, reground for another 30 min, and subjected to a second calcination at 1200 °C for 12 h to enhance crystallinity and phase purity[1]. The final products were finely ground to obtain homogeneous powders suitable for further characterization.

Degradation under Dark and Light Conditions:

The degradation of azo dyes was evaluated under both dark and light irradiation conditions. For each test, 100 mg of catalyst was added to 50 mL of an aqueous azo dye solution (10 mg/L). The mixture was continuously stirred, and at regular intervals, 2 mL aliquots were withdrawn, centrifuged at 4000 rpm to remove the catalyst, and the absorbance of the supernatant was recorded using a UV–Vis spectrophotometer. The degradation efficiency (%) was calculated using:

$$\text{Degradation efficiency (\%)} = [(C_o - C_t)/ C_o] \times 100 \qquad (1)$$

here C_o and C_t represent the pollutant concentration at the initial time and at time t, respectively. Cyclic photocatalytic activity tests were performed using the same procedure. After each cycle, the photocatalyst was recovered, washed with ethanol, dried at 80 °C, and reused with a fresh dye solution.

Estimation of Reactive Oxygen Species (ROS):

Hydroxyl radical (•OH) and superoxide radical ($•O_2^-$) concentrations were determined using terephthalic acid fluorescence and nitroblue tetrazolium (NBT) assays, respectively[2] . For hydroxyl radical detection, 2 mM terephthalic acid (TA) was added to 100 mg of BS or BS4 in 50 mL of deionized water. Samples (2 mL) were collected at intervals, centrifuged, and analyzed for fluorescence at an excitation wavelength of 312 nm. For superoxide radical detection, 50 mL of 0.05 mM NBT solution was introduced under the same conditions. The reaction between $•O_2^-$ and NBT produces mono- and diformazan, indicated by a decrease in absorbance at 259 nm. Samples (2 mL) were collected periodically, centrifuged, and their absorbance was measured with a UV–Vis spectrophotometer.

Text S2. Characterization of catalyst

The synthesized $BaSn_{1-x}Cu_xO_3$ samples were characterized using various analytical techniques. Powder X-ray diffraction (XRD) patterns were obtained on a PANalytical X'Pert[3] diffractometer with Cu Kα radiation (λ = 1.5406 Å). The surface morphology and elemental distribution were examined by field-emission scanning electron microscopy (FE-SEM, Thermo Fisher FEI QUANTA 250) equipped with an energy-dispersive X-ray spectroscopy (EDS) unit, operated at 30 kV. X-ray photoelectron spectroscopy (XPS) measurements were carried out on a Thermo Scientific K-Alpha spectrometer. Fourier transform infrared (FT-IR) spectra were recorded using a Thermo Scientific Nicolet iS10 instrument. The optical bandgap and photocatalytic degradation studies were performed with a UV–Vis–NIR spectrophotometer (JASCO V-670). Hydroxyl radical quantification and electron–hole recombination behavior were investigated using a Hitachi F-7000 spectrofluorometer. High-resolution mass spectrometry (HR-MS) data were collected on a Waters XEVO G2-XS QToF instrument. Specific surface area and pore size distribution were determined via BET and BJH analyses using a Quantachrome ASiQwin system. Electron paramagnetic resonance (EPR) spectra were recorded with a JEOL JES FA200 spectrometer. The total organic carbon (TOC) content of degraded dye solutions was measured using a TOC-L CPN analyzer (Shimadzu).

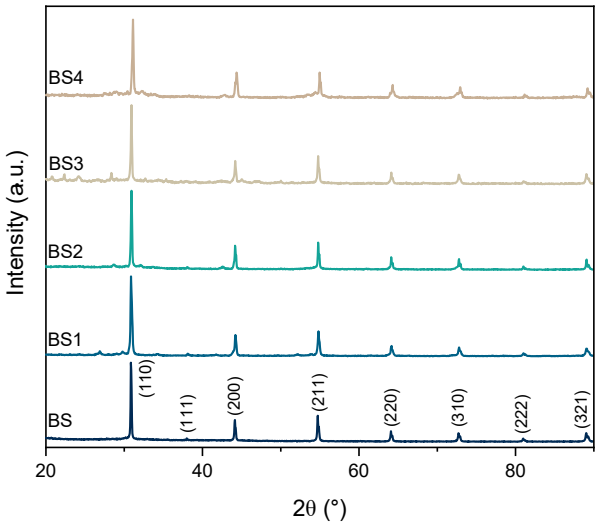

Fig. S1. (a) Powder XRD patterns of BS and BS1-4

Table S1. The percentages of O_L, $O_{V,}$ and O_H of the samples

Samples	O_L (%)	O_V (%)	O_H (%)
BS	57.2	27.5	16.8
BS4	39	39.2	21.5

Text S3. XPS spectra of BS and BS4

Figure S2a presents similar XPS survey spectra for both pure BS and BS4, confirming the presence of Ba, Sn, O, and Cu elements in the photocatalysts. Figure S2b displays the core-level XPS spectra for Ba. For BS, two peaks at 780.6 eV and 795.35 eV correspond to the Ba 3d5/2 and Ba 3d3/2 states, respectively. In contrast, BS4 shows these peaks at 780.02 eV and 795.32 eV. Figure S2c illustrates the Sn 3d spectrum. In BS, the Sn 3d5/2 and Sn 3d3/2 states are observed at 486.67 eV and 495.18 eV, respectively, with a peak separation of 8.51 eV. For BS4, these peaks are found at 486.62 eV and 495.08 eV, exhibiting a binding energy separation of 8.0 eV. Figure S2d illustrates the Cu 2p core level splitting, with the Cu $2p_{3/2}$ state in the BS4 spectrum showing a Cu^{2+} peak at 932.98 eV. This is unequivocally confirmed by the presence of two characteristic shake-up satellites at 942.35 eV and 940.85 eV.

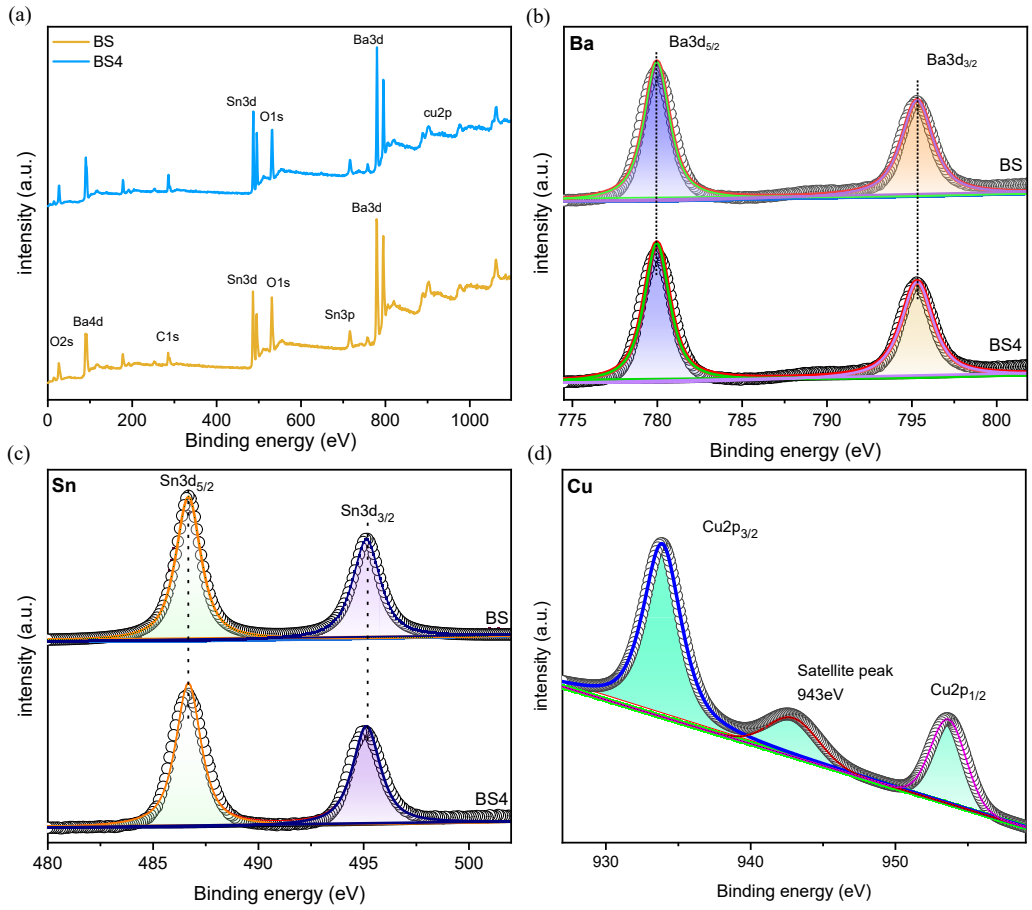

Fig. S2. (a) XPS survey spectrum (b) Ba 3d, (c) Sn 3d and (d) Cu2p of BS and BS4

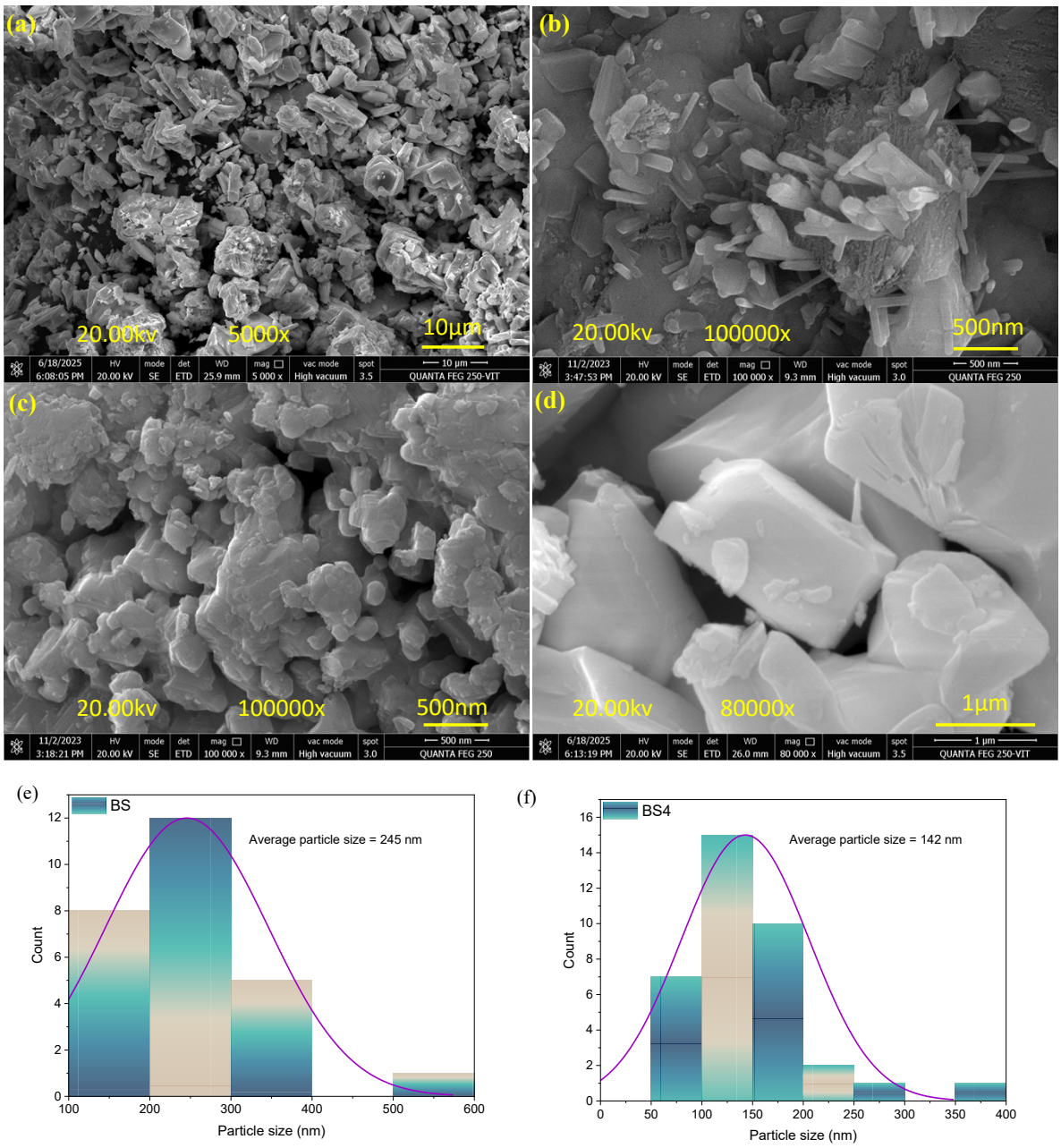

Fig. S3. FESEM image of (a,b) BS, (c,d) BS4 and particle size distribution of (e) BS and (f) BS4

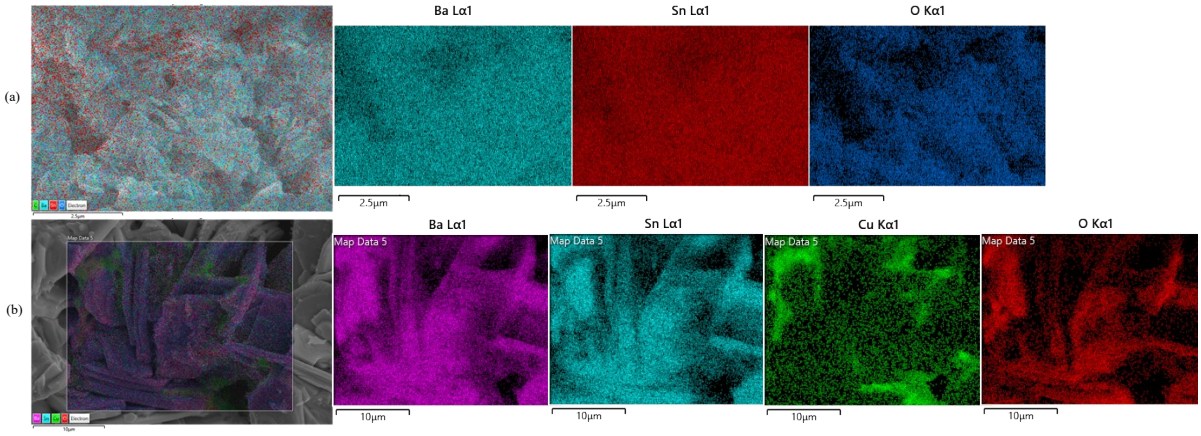

Fig. S4. Elemental mapping of (a) BS and (b) BS4

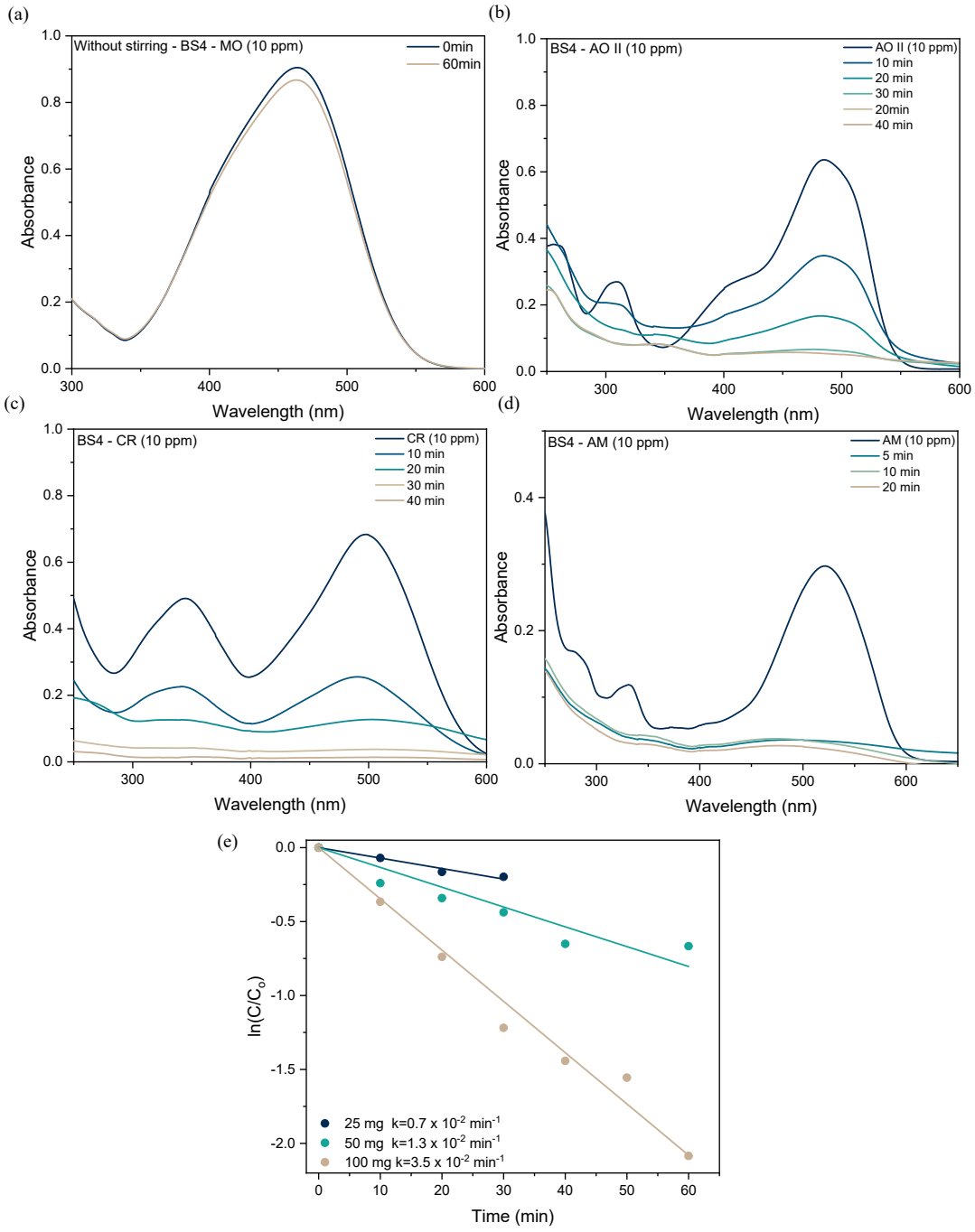

Fig. S5. UV-Vis spectra of (a) Without stirring condition of BS4 with MO (10 ppm), dark degradation (10 ppm) of (b) AO II, (c) CR, (d) AM and (e) kinetics of catalyst dosage variation using BS4 under dark

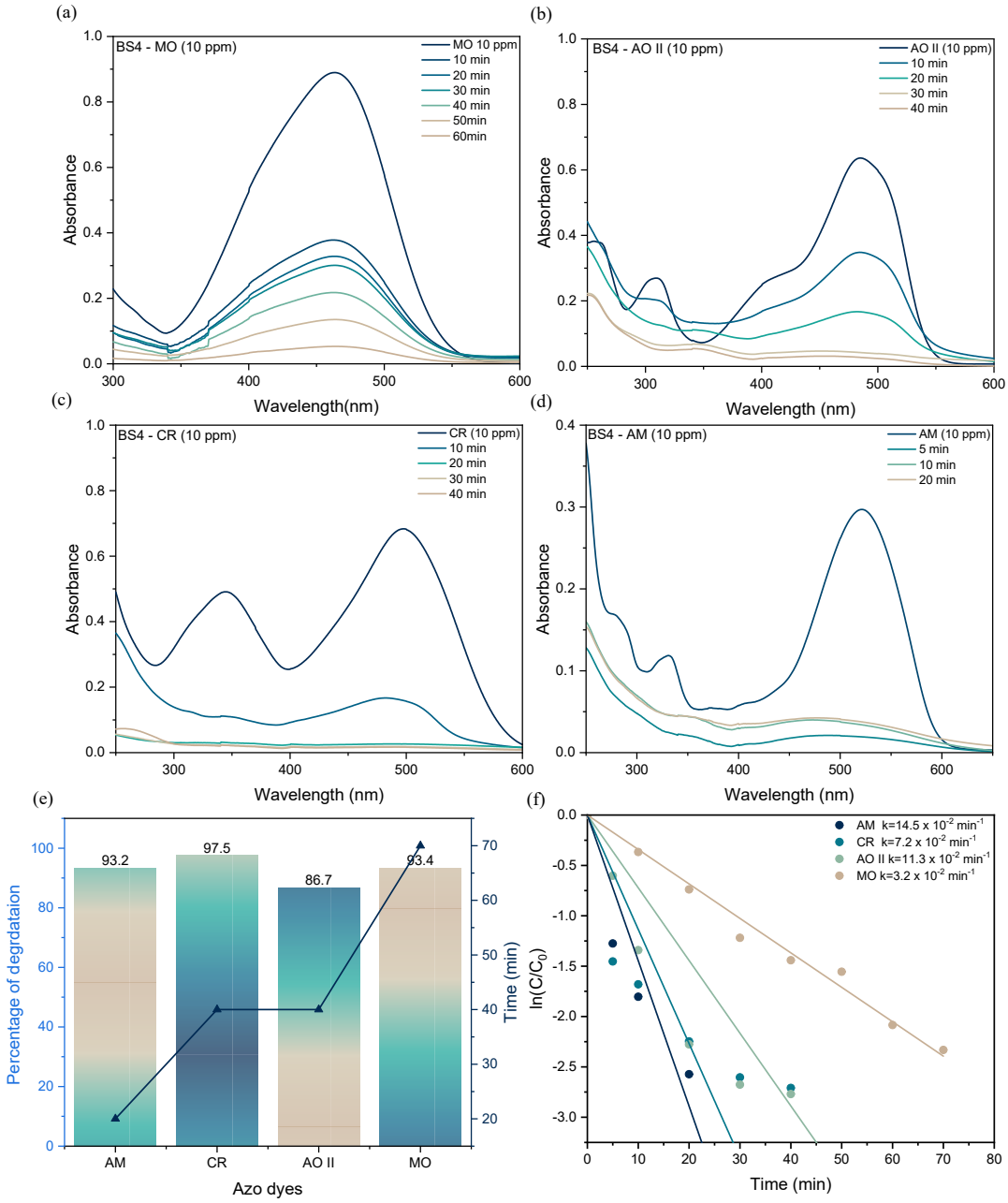

Fig. S6. UV-Vis spectra of (a-d) degradation curve, (e) percentage of degradation and (f) kinetics of MO, AO II, CR and AM using BS4 under ambient conditions

Table S2. Comparison of literature on the degradation of azo dyes in dark

S.No	Catalyst	Catalyst dosage (mg)	Pollutant (ppm)	Degradation (%) (min)	Ref.
1.	La_2NiO_4	75	MO(5)	70 (720)	[3]
2.	$La_4Ni_3O_{10}$	50	MO (5)	98 (210)	[4]
3.	MgSrCoO	200	OA II (20)	89 (480)	[5]
4.	$Ca_xSr_{1-x}CuO_{3-\delta}$ x= 0.75	200	OA II (20)	95 (60)	[5]
5.	$Me_{0.25}Sr_{0.25}Cu_{0.5}O$, Me- Mg & Ce	1 gL^{-1}	OA II (20)	97 (120)	[7]
6.	LaNiO3-δ	150	MO (5)	94.3 (240)	[8]
7.	$CaSrNiO_3$	1 gL^{-1}	OA II (20)	100 (120)	[9]
8.	Ca-Ni-Fe oxides	200	OA II (20)	90 (60)	[10]
9.	Tin-Doped $BiFeO_3$/Graphene	-	CR (100)	89.4 (120)	[11]
10.	Cu-MOF	10	CR (10)	88.1 (30)	[12]
11.	$BaSn_{1.8}Cu_{0.2}O_3$ - Dark	100	MO (10)	85.4 (60)	This work
			AM (10)	91.1 (20)	
			CR (10)	97.2 (40)	
			AO II (10)	93.2 (40)	
12.	$BaSn_{1.8}Cu_{0.2}O_3$ - Ambient	100	MO (10)	86.7 (70)	
			AM (10)	93.2 (20)	
			CR (10)	97.2 (40)	
			AO II (10)	93.4 (40)	

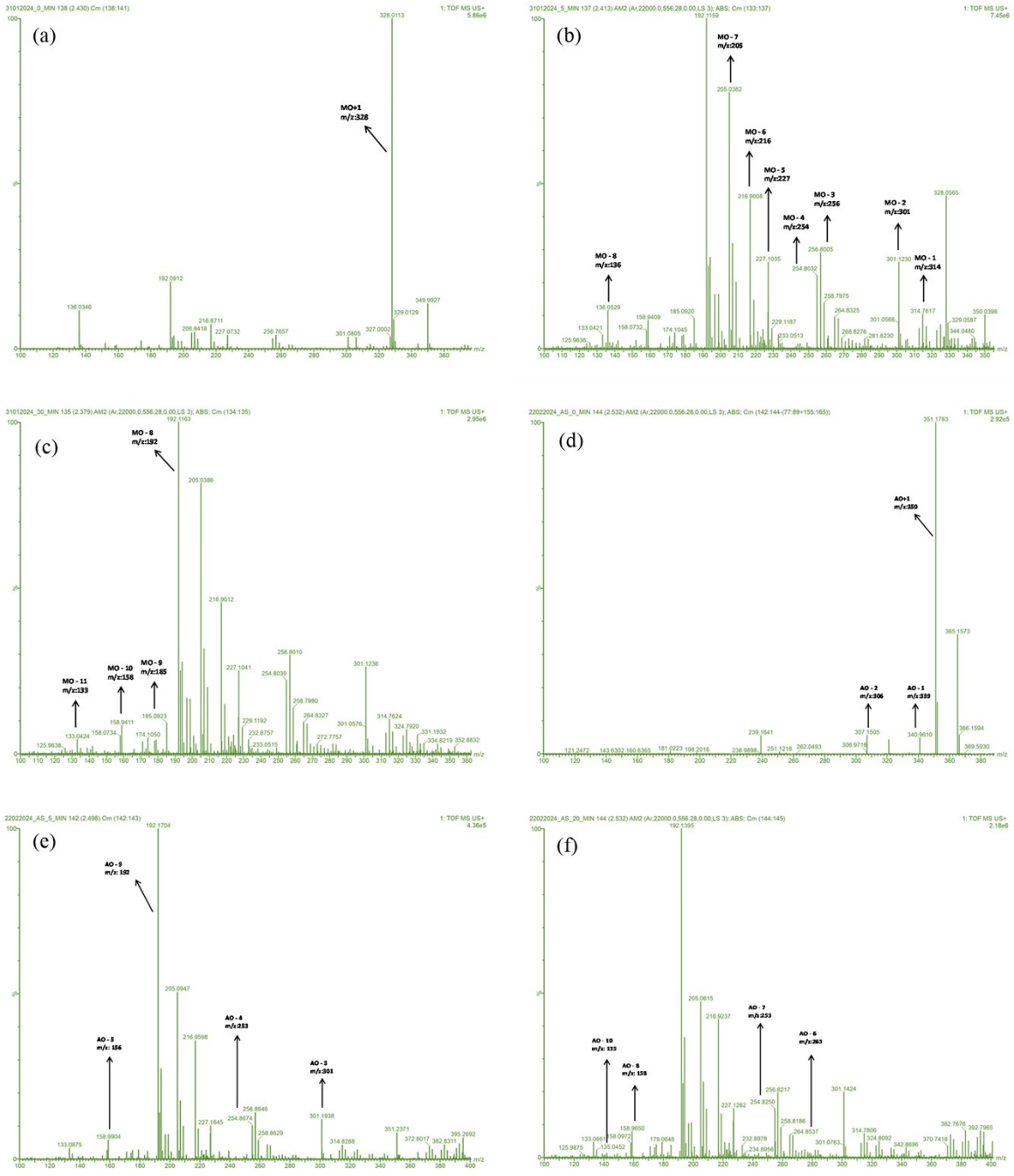

Fig. S7. HRMS spectra of (a-c) MO and (d-f) AO II

Text S4. HRMS Analysis

The degradation of MO, driven by reactive oxygen species (ROS) generated by the catalyst under dark conditions, resulted in the identification of 11 intermediates through HRMS analysis. As illustrated in Fig. S7, the degradation proceeds via three distinct pathways. In Pathway 1, MO (MO+1, m/z = 328) undergoes demethylation at the amino group to yield MO-1 (m/z = 314), followed by desulfonation and sodium ion removal, producing MO-3 (m/z = 256), MO-6 (m/z = 216), and MO-7 (m/z = 205). Pathway 2 begins with MO-2 (m/z = 301), where the azo bond (−N=N−) is reduced to a hydrazo bond (−NH−NH−) accompanied by sodium ion loss. Subsequent N–N bond cleavage generates MO-4 (m/z = 254), MO-9 (m/z = 185), and MO-10 (m/z = 158). In Pathway 3, desulfonation and sodium ion removal yield MO-5 (m/z = 227), which then undergoes benzyl group cleavage to form MO-8 (m/z = 192) and MO-11 (m/z = 133). Similarly, the AO II degradation process, also mediated by ROS, yielded 10 intermediates. Pathway 1 starts with AO+1 (m/z = 350), which loses a hydroxyl group to form AO-1 (m/z = 339). Ring opening and benzyl group cleavage produce AO-3 (m/z = 301), followed by azo bond cleavage to generate AO-4 (m/z = 253) and AO-5 (m/z = 156). Pathway 2 involves desulfonation, hydroxyl removal, and azo bond cleavage, resulting in AO-9 (m/z = 192) and AO-10 (m/z = 135). Pathway 3 begins with the conversion of a sulfonic acid group to a thiol group, forming AO-2 (m/z = 305), followed by hydroxyl and thiol removal to produce AO-6 (m/z = 263), AO-7 (m/z = 254), and AO-8 (m/z = 158). In both degradation systems, the high-molecular-weight intermediates are progressively broken down into smaller molecules, which are ultimately mineralized into CO_2, H_2O, and other harmless products over extended reaction times.

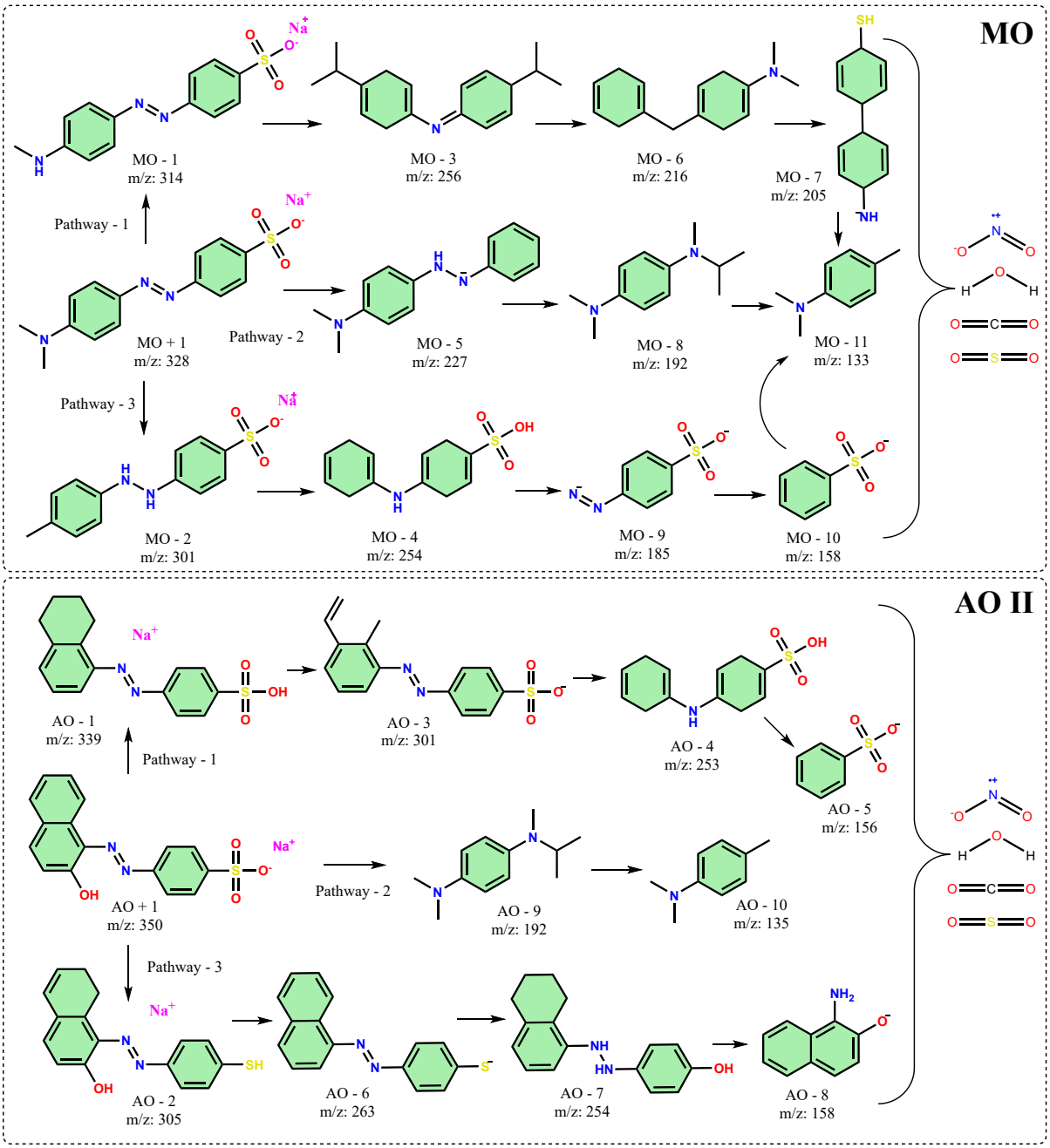

Fig. S8. Plausible mechanism of MO and AO II degradation pathway by BS4 under dark condition

Table S3. ECOSAR software results for acute and chronic toxicity of MO and its photo degradation intermediates towards using three aquatic organisms

PI	Compound Structure	ECOSAR classification	Acute toxicity (mg/L)			Chronic toxicity (mg/L)		
			Fish (LC_{50})	Daphnid (LC_{50})	Green algae (EC_{50})	Fish	Daphnid	Green algae
1.	MO-1	Natural organics	1.51E+4	7.93E+3	4.24E+3	1.35E+3	619	929
2.	MO+1	Natural organics	4.48E+3	2.23E+4	9.68E+3	3.75E+3	1.51E+3	1.89E+3
3.	MO+2	Natural organics	5.69E+4	2.80E+4	1..15E+4	4.70E+3	1.83E+3	2.19E+3
4.	MO+3	Azomethine	0.055	0.095	0.015	0.00047	0.0012	0.014
5.	MO+4	Aliphatic amines	4.00E+3	405	461	381	28.4	136
6.	MO+5	Natural organics	14.6	9.27	11.1	1.63	1.24	3.73
7.	MO+6	Natural organics	0.346	0.260	0.612	0.047	0.055	0.298
8.	MO+7	Natural organics	10.8	6.94	8.59	1.22	0.952	0.95
9.	MO+8	Natural organics	11.7	7.49	9.01	1.32	1.01	3.06
10.	MO+9	Natural organics	5.12E+5	2.24E+5	5.71E+4	3.68E+4	1.06E+4	8.39E+4
11.	MO+10	Natural organics	9.04E+5	3.83E+5	8.53E+4	6.26E+4	1.66E+4	1.16E+4
12.	MO+11	Natural organics	25.2	15.3	15.0	2.66	1.79	4.54

Table S4. ECOSAR software results for acute and chronic toxicity of AO II and its photo degradation intermediates towards using three aquatic organisms

PI	Compound Structure	ECOSAR classification	Acute toxicity (mg/L)			Chronic toxicity (mg/L)		
			Fish (LC_{50})	Daphnid (LC_{50})	Green algae (EC_{50})	Fish	Daphnid	Green algae
1.	AO-1	Natural organics	1.13E+3	769	654	133	82.0	184
2.	AO+1	Natural organics	4.48E+4	2.23E+4	9.68E+3	3.75E+3	1.51E+3	1.89E+3
3.	AO+2	Natural organics	5.69E+4	2.80E+4	1.15E+4	4.70E+3	1.83E+3	2.19E+3
4.	AO+3	Natural organics	1.08E+3	637	553	110	68.9	157
5.	AO+4	Natural organics	3.70E+4	1.85E+4	8.09E+3	3.11E+3	1.26E+3	1.59E+3
6.	AO+5	Natural organics	9.04E+5	3.83E+5	8.53E+4	6.26E+4	1.66E+4	1.16E+4
7.	AO+6	Natural organics	0.058	0.047	0.162	0.0087	0.013	0.096
8.	AO+7	Natural organics	2.26	1.57	2.70	0.280	0.269	1.11
9.	AO+8	Natural organics	210	117	79.6	20.0	10.7	19.9
10.	AO+9	Natural organics	11.7	7.49	9.01	1.32	1.01	3.06
11.	AO+10	Natural organics	25.2	15.3	15.0	2.66	1.79	4.54

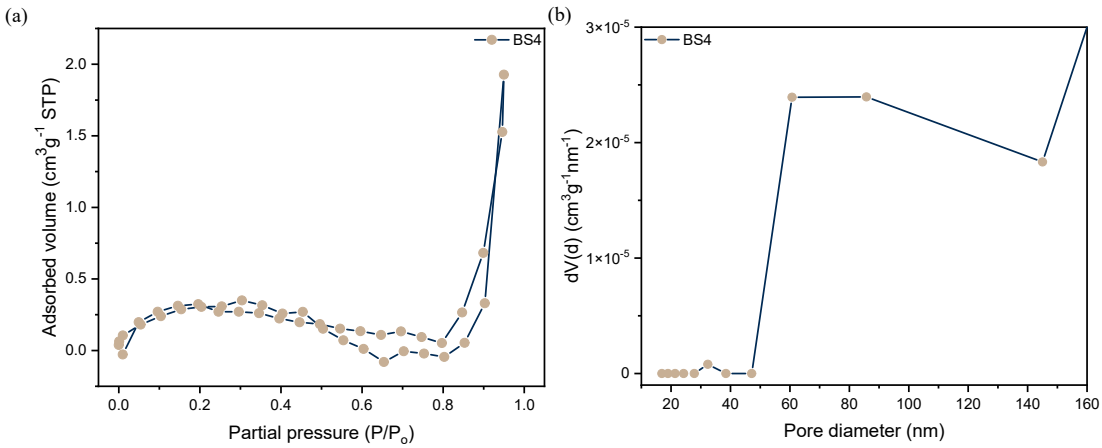

Fig. S9. (a) N_2 adsorption-desorption isotherm (b) pore size distribution of BS4

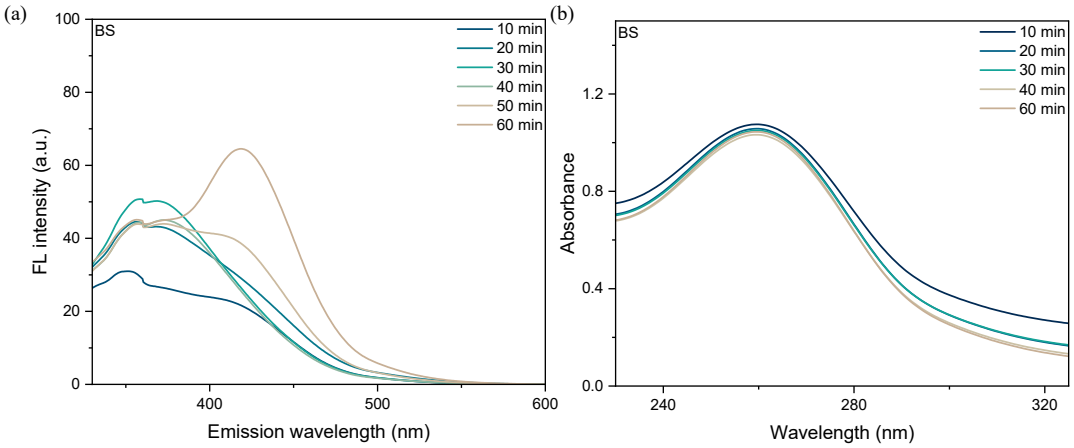

Fig. S10. (a) Fluorescence spectral analysis and (b) degradation study of NBT of BS

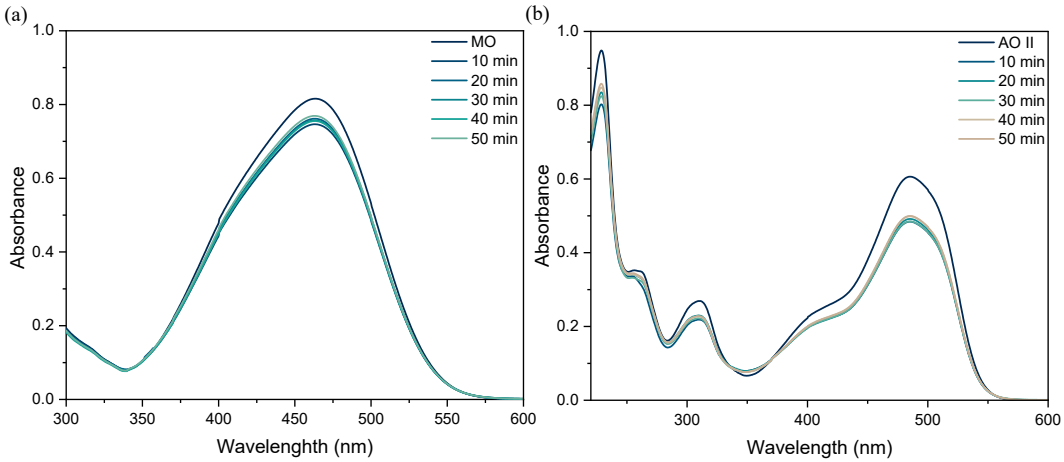

Fig. S11. The degradation curve of (a) MO and (b) AO II dyes using $BaSn_{0.8}Nb_{0.2}O_3$

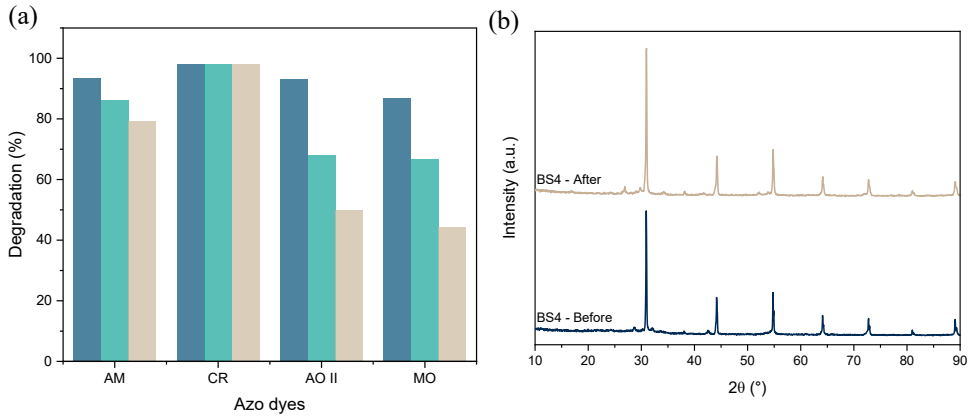

Fig. S12. (a) Recyclability test of BS4 with azo dyes and XRD patterns of BS4 catalyst before and after treatment

References:

1. T. Rohan, D. Harikaran and V. R, *J Environ Chem Eng*, 2025, **13**, 118363.

2. V. Lakshmi Prasanna and R. Vijayaraghavan, *J. Phys. Chem. C.*, 2017, **121**, 18557–18563.

3. G. Li, Y. Zhang, L. Wu, F. Wu, R. Wang, D. Zhang, et al., *RSC Adv.*, 2012, **2**, 4822–4828.

4. JM. Wu and W. Wen. *Environ. Sci. Technol.*, 2010,**44**, 9123-9127.

5. H. Chen, J. Motuzas, W. Martens and J. C. D. da Costa, *Appl. Surf. Sci.*, 2018, **450**, 292–300.

6. H. Chen, J. Motuzas, W. Martens and J. C. D. da Costa, *Appl. Catal. B: Environ.*, 2018, **221**, 691–700.

7. H. Chen, J. Motuzas, W. Martens and J. C. D. da Costa, *Sep. Purif. Technol.*, 2018, **205**, 293–301.

8. W. Zhong, T. Jiang, Y. Dang, J. He, S. Y. Chen, C. H. Kuo, D. Kriz, Y. Meng, A. G. Meguerdichian and S. L. Suib., *Appl. Catal. A: Gen.*, 2018, **549**, 302–309.

9. H. Chen, J. Motuzas, W. Martens and J. C. D. da Costa, *Ceram. Int.*, 2018, **44**, 6634–6640.

10. S. V. Besegatto, A. da Silva, C. E. Campos, S. M. G. U. de Souza, A. A. U. de Souza and S. Y. G. González, *Appl. Catal. B: Environ.*, 2021, **284**, 119747.

11. S. Fatima and S. Rizwan, *ACS Omega*, 2023, **8**, 3736–3744.

12. W. Z. Li, Z. T. Liu, X. S. Zhang, Y. Liu and J. Luan, *Inorg. Chem.*, 2024, **63**, 7034–7044.